

---

# Boxy/peanut bulges : formation, evolution and properties

E. Athanassoula<sup>1</sup>, I. Martinez-Valpuesta<sup>1,2</sup>

<sup>1</sup> Laboratoire d'Astrophysique de Marseille (LAM), Observatoire Astronomique de Marseille-Provence (OAMP), 2 Place Le Verrier, 13248 Marseille, Cédex 04, France.

[lia@oamp.fr](mailto:lia@oamp.fr)

<sup>2</sup> IAC, C/Via Lactea s/n, 38200, La Laguna, Tenerife, Spain.

[inv@iac.es](mailto:inv@iac.es)

**Summary.** We discuss the formation and evolution of boxy/peanut bulges (B/Ps) and present new simulations results. Orbital structure studies show that B/Ps are *parts* of bars seen edge-on, they have their origin in vertical instabilities of the disc material and they are somewhat shorter in extent than bars. When the bar forms it is vertically thin, but after a time of the order of a Gyr it experiences a vertical instability and buckles. At that time the strength of the bar decreases, its inner part becomes thicker, so that, seen edge-on, it acquires a peanut or boxy shape. A second buckling episode is seen in simulations with strong bars, accompanied by a further thickening of the B/P and a weakening of the bar. Quantitatively, this evolution depends considerably on the properties of the halo and particularly on the extent of its core. This influences the amount of angular momentum exchanged within the galaxy, emitted by near-resonant material in the bar region and absorbed by near-resonant material in the halo and in the outer disc. Haloes with small cores generally harbour stronger bars and B/Ps and they often witness double buckling.

## 1 Introduction

Disc galaxies viewed edge-on often show in their central parts a characteristic thickening, which has the shape of a box, of a peanut, or of an 'X' (e.g. [17, 18]). Since these structures swell out of the disc plane, they are called bulges, and more specifically, boxy bulges, or peanut bulges, or 'X' shaped bulges, or, for short, B/Ps or B/P bulges. Yet their properties, as well as their formation and evolution are very different from those of classical bulges [4]. In fact, evidence from many studies has shown that they are just *parts* of bars seen edge-on. Here, we will briefly review relevant results about their orbital structure (Section 2) and describe their formation and evolution as witnessed in  $N$ -body simulations (Section 3). Based on the inner halo structure, we

distinguish different types of models and discuss the role of the halo on the growth of the bar and of the B/P.

## 2 Orbital structure

In order to understand the dynamics of any structure, it is essential to study first the periodic orbits that form its backbone. For two-dimensional bars, the backbone is the well studied family of  $x_1$  orbits [14, 8]. These are elongated along the bar and have an axial ratio that varies both as a function of their Jacobi constant and of the properties of the bar potential used [1]. When stable, they trap around them other orbits. The problem is more complex in three dimensions, since a vertical instability of parts of this family [11] introduces a number of other families extending vertically well outside the disc, such as the  $x_1v_1$ ,  $x_1v_2$ ,  $x_1v_3$  etc. [23, 25, 26, 22]. These families, together with the main  $x_1$  family from which they bifurcate, are known as the  $x_1$  tree. [25]. They are linked to the  $n : 1$  vertical resonances and extend well outside the disc equatorial plane. As shown in [22], some of them are very good building blocks for the formation of B/Ps, because their orbits are stable and have the right shape and extent. Studies of these orbits reproduced many of the B/P properties and helped explaining crucial aspects of B/P formation and evolution. For example, an analysis of the orbital families that constitute B/Ps predicts that they should be shorter than bars. This is indeed verified both in  $N$ -body simulations and in real galaxies ([4], [18], [7]). Furthermore, such studies predict that stronger bars should correspond to stronger B/Ps, and this also is verified both in  $N$ -body simulations ([6] and Athanassoula & Martinez-Valpuesta, in preparation) and in real galaxies ([18]).

## 3 Formation and evolution of boxes and peanuts

The formation of boxy/peanut bulges has been witnessed in a large number of simulations ([12], [13], [24], [9], [3], [4], [21], [15], [19], [16], [20], etc). These have many aspects in common, but also many differences. We will describe and illustrate here two different characteristic types of evolution, corresponding to two simulation types which in [9] have been labelled MH and MD, respectively.

In both cases the simulation starts with an exponential disc of unit mass and unit scale-length. It is immersed in a live halo and the halo-to-disc mass ratio is 5. In MH type models the halo has a small core, smaller or of the order of the disc scale-length, i.e. it is centrally concentrated. Thus, in the disc region, the halo contribution to the circular velocity curve is of the same order as that of the disc. On the contrary, in MD type models the halo has a very big core, much larger than the disc scale length, so that in the inner parts the disc dominates.

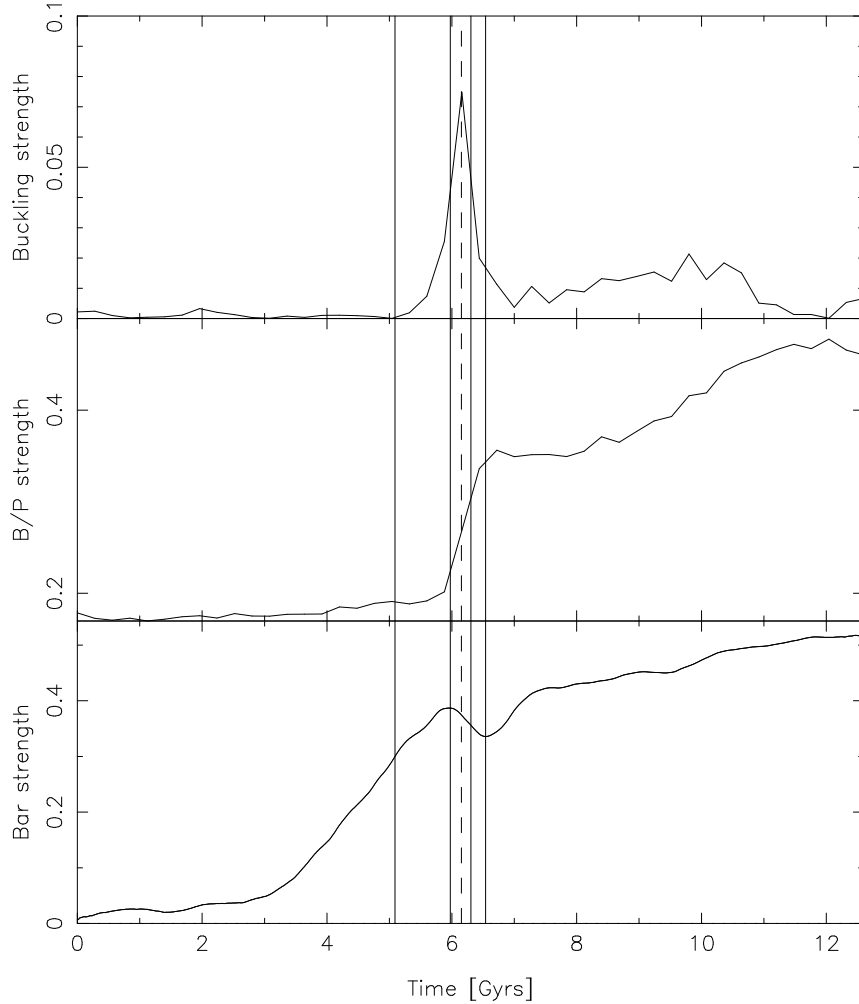
The evolution of the bar in these two types of models is quite different ([9]). In both cases the bar grows by exchanging angular momentum with the outer disc and with the halo. Angular momentum is emitted by near-resonant material in the bar region and is absorbed by near-resonant material in the outer disc and in the halo ([2]). The halo density at the locations of the resonances is much larger in MH types than in MD types. Thus, provided the resonances are responsive, there will be more angular momentum exchanged within the galaxy in MH types than in MD types. This leads to strong bars in MH types and much weaker ones in MD types ([9, 3]).

The time evolution of characteristic properties of the bar and the B/P is shown in Figs. 1, 2 and 3 for two MH and one MD type simulations, respectively. From top to bottom, the panels give the buckling strength, the B/P strength and the bar strength. The time is given in Gyrs, using the calibration proposed in [9]. Fig. 1 shows that the initially unbarred disc forms a bar roughly between times 3 and 6 Gyrs (lower panel). We define as bar formation time the time at which the bar-growth is maximum (i.e. when the slope of the bar strength as a function of time is maximum) and indicate it by the first vertical line in Fig. 1. The bar strength reaches a maximum at a time noted by the second vertical line, and then decreases considerably over  $\sim 0.5$  Gyr. The time at which the bar amplitude decrease is maximum is given by the third vertical line. Subsequently, the bar strength reaches a minimum, at a time shown by the fourth vertical line, and then starts increasing again at a rate much slower than that during bar formation.

The upper panel shows the buckling strength, i.e. the vertical asymmetry, as a function of time. Before the bar forms the disc is vertically symmetric, with the first indications of asymmetry occurring after bar formation. The asymmetry grows very abruptly to a strong, clear peak and then drops equally abruptly. The time of the buckling (dashed vertical line) is very clearly defined as the maximum of this curve. The middle panel shows the strength of the B/P, i.e. its maximum vertical extent, again as a function of time. This quantity grows abruptly after the bar has reached its maximum amplitude and during the time of the buckling. This abrupt growth is followed by a much slower increase over a longer period of time.

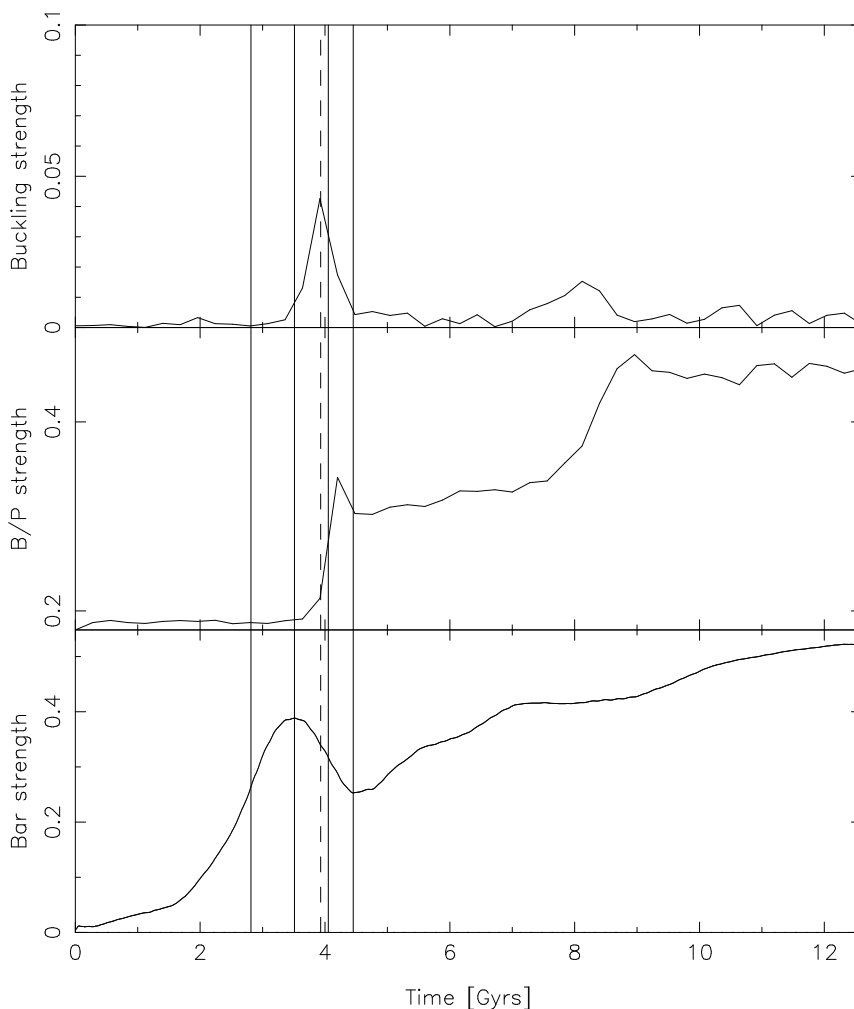
Taken together, the three panels of Fig. 1 show that the bar forms vertically thin, and only after it has reached a maximum strength does the buckling phase occur. During the buckling time the bar strength decreases significantly, while the B/P strength increases. The time interval during which B/P formation, or buckling occur is rather short, of the order of a Gyr, and it is followed by a longer stretch of time during which the bar and B/P evolve much slower.

Fig. 2 shows results for another MH simulation. The first part of the evolution is very similar to that of the previous example, except that the time for bar formation is shorter and the time during which the bar amplitude decreases is somewhat longer. This example, however, has a very interesting feature : it has a second, weaker buckling episode shortly after 8 Gyrs. This occurs very often in simulations developing strong bars and was discussed



**Fig. 1.** Example of the time evolution of three B/P-, or bar-related quantities for an MH type model. These are the buckling strength (i.e. the vertical asymmetry; upper panel), the B/P strength (i.e. its maximum vertical extent; middle panel) and the bar strength (lower panel). The vertical lines mark characteristic times linked to bar formation and evolution. From left to right, these are the bar formation time, the maximum amplitude time, the bar decay time and the bar minimum amplitude time (see text). The vertical dashed line marks the time of the buckling.

first in [5] and [20]. It is seen clearly in all three panels and has characteristics similar to those of the first buckling. Namely, there is an asymmetry, with a clear maximum of the buckling strength, a sharp increase of the B/P strength and a flattening of the bar strength. In many other examples with two buckling episodes, instead of a flattening there is a decrease of the bar



**Fig. 2.** As in Fig. 1, but for an MH-type simulation with two buckling episodes.

amplitude. Thus, the main differences between the two buckling episodes are only that the buckling peak is broader and less high and that the drop in the bar strength is less strong. The time between the two bucklings, in this example, is about 4 Gyrs.

The evolution of the same quantities for the MD simulation is given in Fig. 3. Many crucial differences are immediately clear. The bar forms much faster than for the MH type models, in less than 2 Gyrs. This is in good agreement with results of previous simulations [10, 2]. There is a first maximum of the bar amplitude before 2 Gyrs, which, however, is not associated with a maximum of the asymmetry (buckling), nor with a sharp increase of

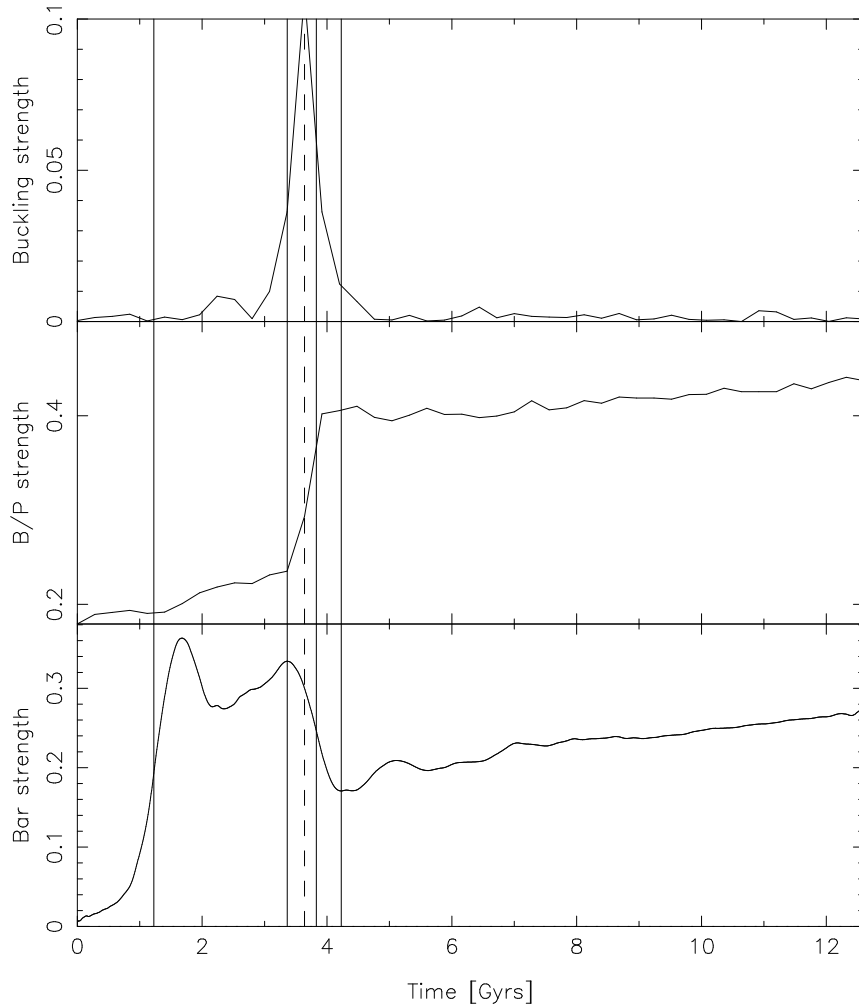


**Fig. 3.** As in Fig. 1, but for an MD-type simulation.

the B/P strength. It thus can not be linked to the B/P formation, and we checked this further by viewing the evolution of the simulation by eye. This revealed that in the initial stages of the simulation a very long and thin bar forms, due to the strong instability in the disc-dominated inner region. This bar drives a strong, two-armed spiral which heats the disc and thus lowers its own amplitude. Furthermore, the bar is so thin that it must render many of the orbits that support it chaotic [8], so that they can not support it further. Thus, the bar strength should decrease spectacularly and this is indeed witnessed in Fig. 3. Subsequently, the bar amplitude increases with time until the formation of the B/P, which, as in the previous examples, is clearly seen

as a maximum of the buckling strength, a sharp increase of the B/P strength and a sharp decrease of the bar strength. The time between the bar growth and its decay is much longer than in the previous examples. In this specific case it is about 2.5 Gyrs, but in other cases it can be considerably longer.

It is thus clear that the halo properties, and in particular the size of its core, influence strongly the time evolution of the bar and of the B/P.

## Acknowledgements

We thank A. Bosma for interesting and fruitful discussions. This work has been partially supported by grant ANR-06-BLAN-0172 and by the Grüber foundation.

## References

1. Athanassoula, E. 1992, MNRAS, 259, 328
2. Athanassoula, E. 2002, ApJL, 569, 83
3. Athanassoula, E. 2003, MNRAS, 341, 1179
4. Athanassoula, E. 2005a, MNRAS, 358, 1477
5. Athanassoula, E. 2005b, in *Planetary Nebulae as Astronomical Tools*, eds. R. Szczerba, G. Stasińska & S. K. Górný, AIP Conf. Proc. 804, Melville, New York, 333
6. Athanassoula, E. 2006, in *Mapping the Galaxy and Nearby Galaxies*, eds. K. Wada and F. Combes, Springer, 47
7. Athanassoula, E., Beaton, R. L. 2006, MNRAS, 370, 1499
8. Athanassoula, E., Bienaymé, O., Martinet, L., Pfenniger, D. 1983, A&A, 127, 349
9. Athanassoula, E., Misiriotis, A. 2002, MNRAS, 330, 35 (AM02)
10. Athanassoula, E., Sellwood, J. A. 1986, MNRAS, 221, 213
11. Binney, J. 1978, MNRAS, 183, 501
12. Combes, F., Sanders, R. H. 1981, A&A, 96, 164
13. Combes, F., Debbasch, F., Friedli, D., Pfenniger, D. 1990, A&A, 233, 82
14. Contopoulos, G., Papayannopoulos, T., A&A, 92, 33
15. Debattista, V. P., Carollo, M., Mayer, L., Moore, B. 2004, ApJ, 604, L93
16. Debattista, V. P., Carollo, M., Mayer, L. Moore, B., Wadsley, J., Quinn, T. 2006, ApJ, 645, 209
17. Lütticke, R., Dettmar, R.-J., Pohlen, M. 2000a, A&AS, 145, 405
18. Lütticke, R., Dettmar, R.-J., Pohlen, M. 2000b, A&A, 362, 435
19. Martinez-Valpuesta, I., Shlosman, I. 2004, ApJ, 613, 29
20. Martinez-Valpuesta, I., Shlosman, I., Heller, C. 2006, ApJ, 637, 214
21. O'Neill, J. K., Dubinski, J. 2003, MNRAS, 346, 251
22. Patsis, P., Skokos, Ch., Athanassoula, E. 2002, MNRAS, 337, 578
23. Pfenniger, D. 1984, A&A, 134, 373
24. Raha, N., Sellwood, J. A., James, R. A., Kahn, F. D. 1991, Nature, 352, 411
25. Skokos, H., Patsis, P., Athanassoula, E. 2002a, MNRAS, 333, 847
26. Skokos, H., Patsis, P., Athanassoula, E. 2002b, MNRAS, 333, 861